ELSEVIER

Radiotherapy and Oncology 71 (2004) 223–234

RADIOTHERAPY & ONCOLOGY
JOURNAL OF THE EUROPEAN SOCIETY FOR THERAPEUTIC RADIOLOGY AND ONCOLOGY

www.elsevier.com/locate/radonline

The use of an aSi-based EPID for routine absolute dosimetric pre-treatment verification of dynamic IMRT fields

Ann Van Esch*, Tom Depuydt, Dominique Pierre Huyskens

Department of Oncology, Division Radiation Physics, University Hospital Gasthuisberg, Herestraat 49, B-3000 Leuven, Belgium

Received 11 March 2003; received in revised form 9 February 2004; accepted 25 February 2004

Abstract

Background and purpose: In parallel with the increased use of intensity modulated radiation treatment (IMRT) fields in radiation therapy, flat panel amorphous silicon (aSi) detectors are becoming the standard for online portal imaging at the linear accelerator. In order to minimise the workload related to the quality assurance of the IMRT fields, we have explored the possibility of using a commercially available aSi portal imager for absolute dosimetric verification of the delivery of dynamic IMRT fields.

Patients and methods: We investigated the basic dosimetric characteristics of an aSi portal imager (aS500, Varian Medical Systems), using an acquisition mode especially developed for portal dose (PD) integration during delivery of a—static or dynamic-radiation field. Secondly, the dose calculation algorithm of a commercially available treatment planning system (Cadplan, Varian Medical Systems) was modified to allow prediction of the PD image, i.e. to compare the intended fluence distribution with the fluence distribution as actually delivered by the dynamic multileaf collimator. Absolute rather than relative dose prediction was applied. The PD image prediction was compared to the corresponding acquisition for several clinical IMRT fields by means of the gamma evaluation method.

Results and conclusions: The acquisition mode is accurate in integrating all PD over a wide range of monitor units, provided detector saturation is avoided. Although the dose deposition behaviour in the portal image detector is not equivalent to the dose to water measurements, it is reproducible and self-consistent, lending itself to quality assurance measurements. Gamma evaluations of the predicted versus measured PD distribution were within the pre-defined acceptance criteria for all clinical IMRT fields, i.e. allowing a dose difference of 3% of the local field dose in combination with a distance to agreement of 3 mm.

Keywords: Intensity modulated radiation treatment; Absolute dosimetric verification; Amorphous silicon electronic portal imaging device

1. Introduction

The use of intensity modulated radiation treatment (IMRT) in clinical routine is spreading rapidly and its advantages in better target coverage in combination with sparing of normal tissue and organs at risk are being explored by more and more centres. The possibility of simultaneously treating different target volumes with different fractionations is opening new possibilities and clinical trials are being started up. IMRT plans become more and more complex: from mildly modulated IMRT prostate fields to highly modulated head and neck fields, even more so when using a combined fractionation scheme. However, a practical drawback on the implementation of IMRT into the clinical routine remains the time consuming patient specific quality assurance (QA) that precedes the actual treatment. The most widely used form of pre-treatment QA for IMRT generally consists of absolute dose measurements (with ionisation chamber, diode, TLD, etc.) combined with isodose distribution measurements in a phantom (film), or even by means of gel dosimetry [24]. The actual data acquisition as well as the data handling for comparison remains a time consuming task [24].

A more efficient tool for pre-treatment QA is the electronic portal imaging device (EPID) as mounted on the linac, providing real-time, digital feedback to the user. For a typical pre-treatment QA scenario by means of a portal imager, two requirements must be met: firstly a proper acquisition mode must be available to detect all dose deposited in the imager during irradiation of the treatment field; secondly one needs to be able to predict what the

* Corresponding author.

0167-8140/$ - see front matter © 2004 Elsevier Ireland Ltd. All rights reserved.
doi:10.1016/j.radonc.2004.02.018

integrated portal dose (PD) image should look like for correct delivery of the fluence distribution.

Research has been performed to predict PD images for portal imaging devices of various types. While there are reports in literature on fluoroscopy-based systems [8,19,20] and on liquid filled ionisation chamber matrices [1,23], there is very little on the relatively new amorphous silicon (aSi) based systems. Some of the published algorithms describe the use of an EPID for absolute dose measurements [9,18–20] but most of the literature is devoted to static fields rather than dynamic dose delivery and to relative rather than absolute dosimetry [2,4,5,8,11,16,19,21,23]. Over the last few years, aSi detectors have become increasingly popular for online portal imaging, requiring less excess dose to be delivered to the patient per portal image and yet yielding a superior image quality than, e.g. the liquid filled ionisation chamber EPID.

An extensive investigation of the dosimetric characteristics of a small (96×96 mm^2) aSi flat panel detector was performed by Munro and Bouius [4,14,17]. They measured the linearity, spatial resolution, glare, noise and signal-to-noise characteristics of an indirect aSi EPID construction, containing a metal plate/phosphor screen generating optical photons that are detected by the photodiodes. El-Mohri et al. [4] studied the characteristics of a similar (albeit somewhat larger) aSi flat panel imager using two detection configurations of the array: the indirect configuration as described by Munro et al. and a direct configuration in which the phosphor screen is absent and radiation is directly sensed by the photodiodes. The sensitivity of the indirect system was considerably higher than that of the direct system, but the latter exhibited dosimetric behaviour similar to the data obtained with an ionisation chamber, whereas the former showed significant differences. For predicting the PD distribution in such an indirect aSi detector, McCurdy et al. explored a two step algorithm [14,15]. Although portal dosimetry for static fields is certainly of interest, the gain would be larger when applicable for dynamic IMRT, even more so when it can be used for absolute dose verification. A recent publication by Greer and Popescu [6] investigates the dosimetric properties of an aSi EPID using a continuous frame-averaging acquisition mode and a 6 MV radiation beam. They concluded the aSi EPID to show promise as an efficient verification tool for IMRT delivery, the main limitations being related to the dead time in the frame acquisition and sensitivity calibration.

We have investigated the characteristics of an aSi portal imaging device equipped with a new acquisition mode for dosimetry applications. We have modified the commercially available single pencil beam dose calculation algorithm (Cadplan/Eclipse) to predict the PD distribution at the level of the detector. The prediction algorithm uses beam data acquired with the portal imager (through the use of the dosimetric acquisition mode) instead of with an ionisation chamber in water. In order to reduce the workload connected to pre-treatment QA to a minimum, we have focused on measuring and predicting absolute rather than relative dose distributions, hence eliminating the need for supplementary point dose measurements.

2. Materials and methods

2.1. The aSi-based EPID for dosimetry in dynamic mode

The EPID used in our study is a commercially available aSi imaging device (aS500, Varian Medical Systems), mounted on a Clinac 2100 C/D (photon energies of 6 and 18 MV) with dynamic MLC (80 leaves) (Varian Medical Systems). The EPID system includes (i) an image detection unit (IDU), featuring the detector and accessory electronics, (ii) an image acquisition unit (IAS2), containing drive and acquisition electronics and interfacing hardware, and (iii) a dedicated workstation (PortalVision PC) located outside the treatment room. The IDU is essentially a matrix of 512×384 pixels with a resolution of 0.784×0.784 mm^2 and a total sensitive area of $\sim 40 \times 30$ cm^2. Each pixel consists of a light sensitive photodiode and a thin film transistor to enable readout. The electric charge generated by the incident photons is accumulated in the photodiode until the signal is read out and digitised through an analogue to digital converter. Overlying the array is a scintillating layer (gadolinium oxysulphide) and a copper plate (of ~ 1 mm thickness) [17], making the portal imager an indirect detection system. The phosphor scintillator converts incident radiation into optical photons, enhancing the sensitivity of the detector more than tenfold [4]. The total water-equivalent thickness of the construction materials in front of the photodiodes is 8 mm, as specified by the manufacturer. The IAS2 controls and reads the IDU. Its local hard disk contains the correction images (i.e. the dark and flood field acquisition) and the various acquisition parameter sets. In order to be able to detect all dose delivered to the portal imager during delivery of the treatment field, a special acquisition mode was used [12,13]. During delivery, a continuous acquisition of frames is obtained. Each frame is read out line by line. The acquisition CPU (ACPU) contains a 14 bit A/D converter and is capable of adding 64 frames in its 20 bit hardware adder. Therefore, a transfer of the frame buffer to the CPU is mandatory after every 64th frame. This introduces a readout interrupt of ~ 0.164 s, as stated by the manufacturer and confirmed by our measurements. The interrupt occurs at regular time intervals of 64 times the acquisition time per frame (e.g. every $64 \times 0.111 = 7.104$ s for 300 MU/min). However, charge accumulation in the photodiode is not interfered with and it will thus not affect the final image accuracy, provided the accumulated charge between two subsequent readouts does not drive the 14 bit A/D converter into saturation. Possible saturation and its impact on the dosimetric accuracy is considered in the next paragraph. The dosimetric acquisition mode foresees an additional

frame readout after the beam has been switched off in order not to neglect the dose delivered to the part of the detector that had already been read out during the acquisition of the last frame with the beam on. The image stored at the CPU is averaged over all acquired frames.

The conversion of the averaged gray-scale image into a PD image is done automatically in the dosimetric workspace of the PortalVision software. Firstly, it is multiplied by the total acquisition time. This time period, noted in the acquisition record, exceeds the beam-on time by 1–2 frame readouts as explained above. Secondly, a correction for the beam profile is applied. Although the standard dark field correction is applied, during the standard flood field calibration of the imager, the beam profile is assumed to be perfectly flat. This being a reasonable approximation for clinical imaging purposes, it introduces errors of a few percent into the dosimetric image. Hence it is corrected for by means of a two-dimensional field profile correction matrix as measured with film (Kodak EDR). The film was irradiated with a $27.5 \times 20.7\ cm^2$ field (i.e. the field size required to cover the entire detector surface at SDD = 145 cm) at isocentre and at a depth of 8 mm. The size of the EDR film did not permit a measurement at source-to-detector distance SDD = 145 cm. The measured two-dimensional dose matrix was subsequently rescaled to SDD = 145 cm, normalised to the beam axis and resampled to the detector grid, resulting in the field profile correction matrix. Thirdly, provided an absolute calibration of the imager has been performed, the image is multiplied with the calibration factor yielding what is referred to as the PD image. The PD image is expressed in calibrated units (CU). All PD image data used in this paper are obtained in this manner.

Furthermore, if not stated otherwise, all data were acquired with the commercially available detector as such, i.e. without any additional build-up placed onto the detector surface.

It may be worthwhile to state that the used dosimetry workspace was made available as a research/developmental tool, rather than for routine clinical use. The year's experience described below may therefore differ from that of users of the final product.

2.2. Dosimetric characteristic of the aSi-based EPID

2.2.1. Detector saturation

Although the capacitance of each photodiode is adequately large to ensure charge accumulation during subsequent readouts, saturation may arise during the A/D conversion. Since the 14 bit A/D component converts the analogue signal from the pre-amplifiers into signed 13 bit values, saturation occurs for pixel counts exceeding an absolute value of 8192 (including the dark field pixel count). We have investigated the limits beyond which saturation starts to occur for a linac calibrated to yield 1 cGy/MU at the isocentre at 10 cm depth for a $10 \times 10\ cm^2$ field. The time per frame readout and the average pixel counts per frame were monitored for all dosimetric acquisition parameter sets (i.e. for all linac dose rate settings, for 6 and 18 MV) at SDD = 145 cm. The acquisition parameter values were set according to the manufacturer's specifications. The field size was set to cover the entire detector surface. Images were obtained with 20 MU, requiring less than 64 frame acquisitions for all linac dose rate settings (ranging from 100 to 600 MU/min). The total signal expected during the frame transfer was calculated assuming the signal accumulation time to be the sum of the time per frame readout and the signal transfer time (0.164 s). The exact detector saturation will vary slightly depending on the dark field correction, the latter typically being in the order of 200 cts/pixel. We have therefore estimated the dosimetric inaccuracy due to detector saturation by applying a fixed pixel saturation of 8000 cts. The same calculations were repeated for SDD = 105 cm, starting from average pixel counts per frame extrapolated from the measurements at SDD = 145 cm using the inverse square law. An estimate of the final dosimetric error due to detector saturation is calculated from the difference between the total required signal and the corresponding maximum detectable signal taking into account saturation beyond 8000 cts/frame for a set of 65 acquired frames. The total required signal is calculated to be 64 times the required average frame pixel count, plus the pixel count expected after the 64th frame transfer. The maximum detectable signal is derived analogously, except that all required pixel counts beyond saturation are truncated at 8000 cts.

2.2.2. Linearity

The linearity of the detector response with dose rate and with frame averaging has been reported in literature [4,14,17]. The maintaining of this linearity through measurement with the above described dosimetric acquisition mode and the subsequent conversion to integrated PD was verified with two measurement series for each accelerator energy. Measurements were performed with the linac dose rate set at 300 MU/min, this being the dose rate used in clinical routine. Firstly, a static field of $10 \times 10\ cm^2$ was delivered with a total amount of monitor units (MU) ranging from 2 to 300 MU at 300 MU/min, at SDD = 145 cm. Secondly, the independence of the signal acquisition as a function of dose rate was verified by monitoring the signal on the beam axis for a static $10 \times 10\ cm^2$ field with 100 MU at different detector positions (ranging from 105 to 180 cm). For the second test, measurements were also performed with an ionisation chamber (PTW-Freiburg, type 61002, 0.125 cm^3) in a 3 cm thick solid water phantom at 8 mm depth for comparison.

2.2.3. Calibration and reproducibility

The detector is calibrated to yield a PD of 1 CU for a $10 \times 10\ cm^2$ field and a dose of 100 MU at SDD = 100 cm. Since in practice, the SDD cannot be reduced beyond

105 cm when the robotic arm is in clinical mode, the actual calibration was performed at SDD = 145 cm, setting the PD to be 0.4756 CU (i.e. assuming inverse square law behaviour). The larger source to detector distance was chosen to avoid all possible detector saturation effects in the calibration.

Day-to-day and long term absolute reproducibility were assessed by means of one static field as well as one dynamic field delivery, using the same two fields over a period of 12 months. The PD image acquisition of these two treatment fields was repeated once a week. Every session encompassed the acquisition of two images per treatment field (i.e. two images of the static and two images of the dynamic treatment field). Dosimetric calibration of the imager, including dark and flood field corrections and an absolute calibration measurement, was performed every 4 months.

2.2.4. Ghosting

To assess the existence of a memory effect of the aSi detector, also referred to as 'ghosting', 500 MU (6 MV) were delivered to the portal imager in a $5 \times 5\ cm^2$ static field, immediately followed by delivery of 10 MU (6 MV) in a $15 \times 15\ cm^2$ static field, during which a dosimetric image was acquired. The dosimetric contribution of the small field delivery to the large field dosimetric acquisition was quantified through comparison with a reference PD image of a $15 \times 15\ cm^2$ field (10 MU) without foregoing irradiation. The test was repeated for 18 MV.

2.2.5. Field size dependence

The field size dependence of the detector signal was assessed at SDD = 105 and 145 cm, for field sizes ranging from 3×3 to $25 \times 25\ cm^2$ for SDD = 105 cm and to $20 \times 20\ cm^2$ for SDD = 145 cm. The dose on the beam axis—averaged over 6×6 pixels—was compared to the dose measured in water at a depth of 8 mm. The measurements in water were performed with the ionisation chamber (PTW-Freiburg, type 61002, $0.125\ cm^3$) positioned on the beam axis at the corresponding SDD and at a depth of 8 mm. Furthermore, the applicability of the concept of equivalent square fields to the aSi detector was assessed through measurement of the dose on the beam axis for rectangular fields at SDD = 145 and 105 cm, with the X collimator position ranging from 3 to 35 cm and the Y collimator position ranging from 3 to 25 cm.

2.2.6. Portal depth dose

The behaviour of the PD as a function of the amount of build-up onto the detector surface (polystyrene, ranging from 0 to 7.6 cm) was measured for both energies. The protective cover was removed in order to reduce the air gap between the flat panel detector and the additional build-up to a minimum (i.e. ~1 mm). The detector surface remained at a fixed SDD (145 cm) as build-up was placed on top (in addition to the 8 mm build-up inherent to the detector system). The PD on the beam axis was averaged over a central region of interest, consisting of 6×6 pixels. Comparative measurements were performed in a water phantom with an ionisation chamber (PTW-Freiburg, type 61002, $0.125\ cm^3$) positioned on the beam axis at a distance of 145 cm; the amount of water above the ionisation chamber was increased up to a depth of 14.5 cm. A field size of $10 \times 10\ cm^2$ was applied for all measurements.

2.3. Portal dose image prediction

The aim of the pre-treatment verification of the dynamic IMRT fields by means of a portal imager is to assess the accuracy of the intended fluence—as used in the TPS for dose calculation—versus the actually delivered fluence through the dynamic leaf motion. Furthermore, the aim is to do so in an absolute way, making any additional (e.g. point dose) measurement unneeded. Since it is impossible to directly measure fluence with this detector system and detector response inevitably affects the incoming fluence measurement, a PD image prediction algorithm is mandatory to compare the theoretically expected measurement to the actual measurement.

The PD prediction algorithm for the aSi measurement is based upon the single pencil beam dose calculation algorithm as originally developed by Storchi et al. [22] and as adapted into the Cadplan TPS (Varian Medical Systems) dose calculation. The TPS dose calculation algorithm is described in detail in the Vision Users Documentation made available by the manufacturer, so only details relevant to the current PD prediction algorithm are presented here. The PD prediction algorithm differs from the Cadplan algorithm in the sense that, in order to predict a fluence measurement with the portal imager, it uses beam data measurements with the portal imager rather than ionisation chamber measurements in water. Furthermore, it does not require modelling of the depth dependence since we are focussing on image prediction at a fixed depth (i.e. in the commercially available portal imager as such).

In analogy to the single pencil beam algorithm in Cadplan, the absolute PD calculation per monitor unit can be separated into the phantom scatter and collimator scatter. Since the Varian MLC is a tertiary collimator, it can be considered as block replacement. Hence, the collimator scatter solely depends on the position of the main collimators. The scatter within the detector, i.e. the equivalent of the phantom scatter in the TPS dose calculation algorithm—is determined by the incoming fluence distribution. The predicted PD image per MU for a field with collimator opening X,Y and intended, theoretical fluence $F(x, y, \mathrm{SDD})$ can then be written as

$$\mathrm{PD}(x, y, \mathrm{SDD}) = \{(F(x, y, \mathrm{SDD}) \cdot \mathrm{OAR}(\mathrm{SDD}) * \mathrm{RF}_{\mathrm{PI}}\} \mathrm{CSF}_{\mathrm{XY}} \frac{1}{\mathrm{MUfactor}} \quad (1)$$

The imager distance at which the measurement is going to

be performed must be known at the time of image prediction, since the theoretical fluence and the beam profile correction (i.e. the off-axis ratio OAR) need to be rescaled accordingly. The theoretical fluence distribution as produced by the TPS is defined at isocentre and has a resolution of $0.25 \times 0.25\ \text{cm}^2$. The first term of Eq. (1) describes the effect of the detector response function RF_{PI}. It is the point spread function or the equivalent of the single pencil beam kernel describing phantom scatter in the TPS dose calculation. The second term holds the collimator scatter factor CSF, solely dependent on the collimator opening. The theoretical fluence matrix as generated by the leaf motion calculator in the Cadplan/Helios software is normalised so that the maximum fluence is equal to unity. A value 1 corresponds to the fluence that would be delivered with a fully open field. The MUfactor, like a wedge factor, is an efficiency factor describing the surplus beam-on time required due to the leaf motion [7]. Therefore, the final image has to be divided by the MUfactor in order to obtain the prediction per MU.

The collimator scatter factor cannot be measured by the portal imager in a direct way, but can be derived from the measured output factor and the calculated phantom scatter factor. The latter is derived from convolving the open beam fluence F_{XY} with RF_{PI}, and monitoring the resulting value on the central axis

$$\text{CSF}_{\text{XY}} = \frac{\text{OF}_{\text{XY}}}{\text{PSF}_{\text{XY}}} = \frac{\text{OF}_{\text{XY}}}{(F_{\text{XY}}\text{RF}_{\text{PI}})_{\text{CAX}}} \tag{2}$$

The output factor OF_{XY} is normalised to the PD per MU of a 10×10 field at $\text{SDD} = 100$ cm, i.e. $\text{OF}_{10\times10}$ $(100\ \text{cm}) \equiv 0.01$ CU.

Essential to the quality of the portal image prediction is the accurate modelling of the portal imager response function. We have opted to take the resolution of the actual fluence already into account when modelling the RF_{PI}. The optimal RF_{PI} was obtained through a least square fit of the PD prediction to a PD measurement of a test plan especially developed for this purpose. The test plan consists of a fluence distribution as produced by the leaf motion calculator from an artificially created pyramid-like optimal fluence matrix (Fig. 1). This fluence was carefully validated by means of film measurements in a phantom and subsequently delivered to the portal imager. The analytical function describing the RF_{PI} as a function of radial distance r from the pencil beam, is modelled as a sum of three Gaussian contributions

$$\text{RF}_{\text{PI}} = \sum_{i=1}^{3} w_i \text{e}^{-\left(\frac{r}{k_i}\right)^2} \qquad \text{with} \qquad \sum_{i=1}^{3} w_i = 1 \tag{3}$$

During the fit procedure, the Gaussian parameters in Eq. (3) are adjusted iteratively until the difference between the predicted dose image (Eq. (1)) and the measured test image is minimised. We make use of the Fast Fourier transform to derive the optimal RF_{PI}. Since the use of Fast Fourier transform requires that both functions are in Cartesian coördinates of the same resolution, the RF_{PI} is sampled from the radially symmetric analytical function in Eq. (3) to match the resolution of the fluence matrix rescaled to the correct SDD. This resampling is performed for every iteration in the fit procedure. Hence the optimal fit parameters inherently take the discretisation into account. Fit parameters were derived for both energies and $\text{SDD} = 105$ and 145 cm.

The PD image prediction was subsequently tested for both energies and both source to detector distances on a series of clinical dynamic IMRT treatment fields. Fields over a large range of collimator sizes were used (ranging from 4×4 to $12 \times 39\ \text{cm}^2$), including strongly as well as mildly modulated fluence distributions. Measured and predicted PD images were compared by means of line profiles and via the gamma evaluation algorithm [3,10]. The gamma matrix was calculated with the algorithm as proposed by Depuydt et al., requesting a distance-to-agreement (DTA) of 3 mm and a maximum dose difference of 3% of the local dose. To assure an identical DTA criterion for all SDD, all images were backprojected to isocentre for the gamma evaluation. A conformity index was defined to be the ratio of the amount of points that fall within the acceptance criteria to the total amount of evaluated points. To obtain a clinically relevant value, only points exceeding a dose of 5% of the maximum field value were taken into account for the calculation of the conformity index.

3. Results

3.1. Dosimetric characteristics of the aSi-based EPID

3.1.1. Detector saturation

The measured acquisition time per detector frame is given in Table 1 for both energies and for all linac dose rate settings. The measured average signal per frame is always well below saturation when measured at $\text{SDD} = 145$ cm. Small dosimetric errors—ranging from 0.35 to 1.4%—are introduced due to saturation of the 65th frame for dose rates beyond 400 MU/min for 6 MV and beyond 500 MU/min for 18 MV. When the detector is positioned as close as possible to the isocentre, saturation effects are predicted for the 65th frame for almost all acquisitions, except for the lowest dose rate settings: 100 MU/min for 6 MV and 200 MU/min for 18 MV. More importantly, for the highest dose rates (i.e. beyond 500 MU/min for 6 MV, for 600 MU/min for 18 MV) saturation even becomes an issue in the standard frame acquisition (i.e. for frames 1–64), introducing errors between 9 and 25%. Although the errors originating from the standard frame and 65th frame saturation are combined into a single value in Table 1, their effect on the dosimetric image can only be combined as such in case of a static field delivery. In case of an IMRT field, the dosimetric

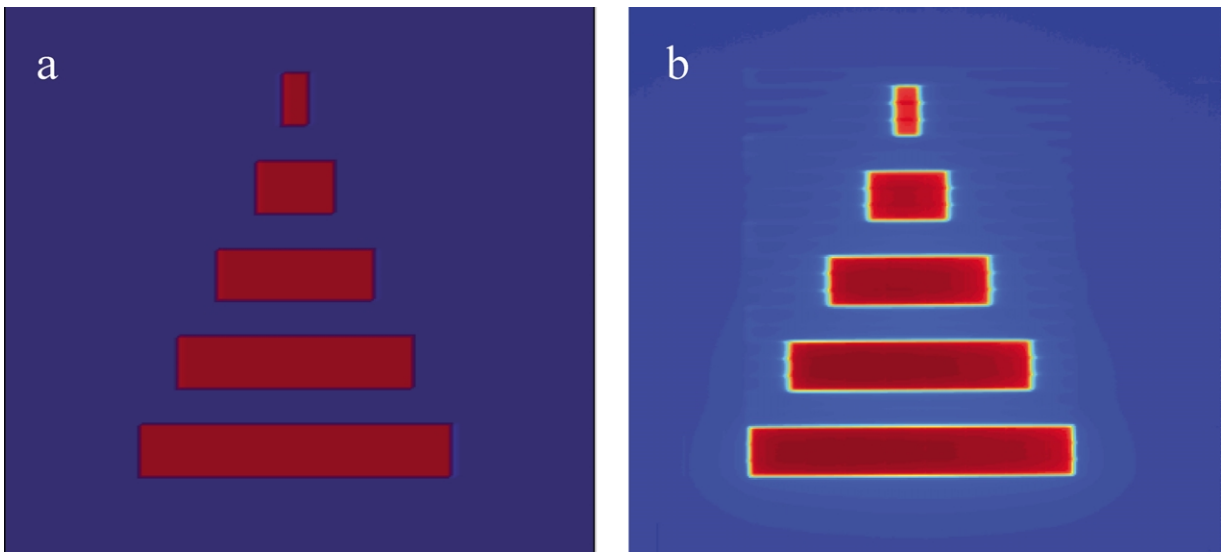

Fig. 1. Pyramid-shaped theoretical test fluence pattern (a) and measured portal dose distribution (b) for the empirical derivation of the portal imager response function. The collimator opening is 12×25 cm^2, the displayed measurement was acquired with 18 MV at SDD = 105 cm.

information that is lost due to detector saturation varies significantly according to the specific interval in which signal was lost. Typical distortions of the portal image due to detector saturation are displayed in Fig. 2. The dynamic

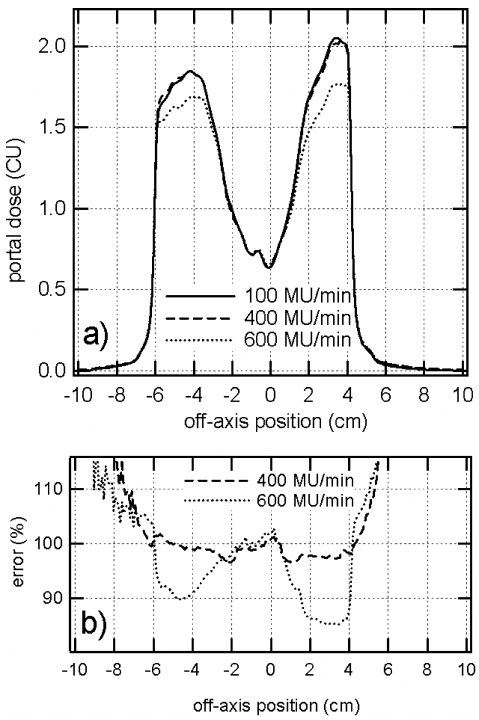

Fig. 2. (a) Line profiles extracted from the absolute portal dose detection of a dynamic field delivery (anterior field of prostate IMRT treatment) with 6 MV at SDD = 105 cm. No saturation effects are present in the image acquired with a dose rate of 100 MU/min, minor discrepancies are present at 400 MU/min, whereas unacceptable distortions (i.e. by large exceeding the gamma evaluation criteria of 3%, 3 mm) are noticeable at 600 MU/min. (b) Relative distortions, i.e. the ratio of the line profiles for 400 and 600 MU/min to the line profile at 100 MU/min.

treatment field was delivered with 6 MV at SDD = 105 cm, with subsequent dose rate settings of 100 (no saturation), 400 (saturation in the 65th frame) and 600 MU/min (saturation in all frames). Deviations due to the saturation of the 65th frame are minor at low dose rates, in contrast to the near-total deformation of the line profile at 600 MU/min.

3.1.2. Linearity

The linearity of the detector response using the dosimetric acquisition mode is illustrated in Fig. 3. The detected PD is proportional to the amount of MUs, over the entire measured range from 300 down to 2 MU. Above 30 MU, the measured PD is within 2% of the expected value, while below 30 MU the accuracy decreases gradually down to 6% of the expected value due to the very low expected signal and the limited number of significant digits in the PD image display: since the PD is only displayed with an accuracy of 0.001 CU, an expected PD of, e.g. ~0.0095 CU at SDD = 145 cm for a 2 MU delivery, will automatically be displayed as 0.010, i.e. with a 5% rounding error. Fig. 3 shows the maintaining of the linearity as a function af physical dose rate due to the varying detector distance. The PD on the beam axis agrees within 2% with the ionisation chamber measurements and within 1% with the inverse square law behaviour (as indicated by the straight line).

3.1.3. Reproducibility

Short term as well as long term detector reproducibility was found to be within 2%, for static as well as dynamic field delivery. Day to day fluctuations in the output of the accelerator were not corrected for and are thus encompassed in the reported value. Similar findings were reported in literature [4,6].

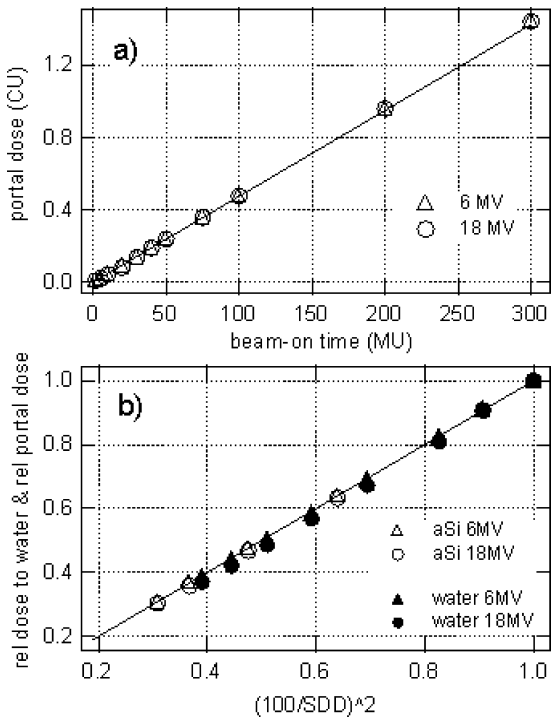

Fig. 3. (a) Portal dose dependence on the beam axis as a function of beam-on time, measured at SDD = 145 cm for a field size of 10×10 cm^2 (6 and 18 MV). (b) Inverse square law behaviour, measured for a field size of 10×10 cm^2 with the aSi detector and with an ionisation chamber in water at 8 mm depth, for varying SDD. The solid lines in both graphs represent ideal linearity.

3.1.4. Ghosting

Fig. 4 shows the remnants of a foregoing irradiation of a small 5×5 cm^2 field with 500 MU in the PD image of a larger static field acquired with 10 MU as soon as physically possible (typically 10 s) after the delivery of the small field. The ratio of both line profiles (insert of Fig. 4) displays a signal remnant below $\sim 1\%$ for 6 and 18 MV.

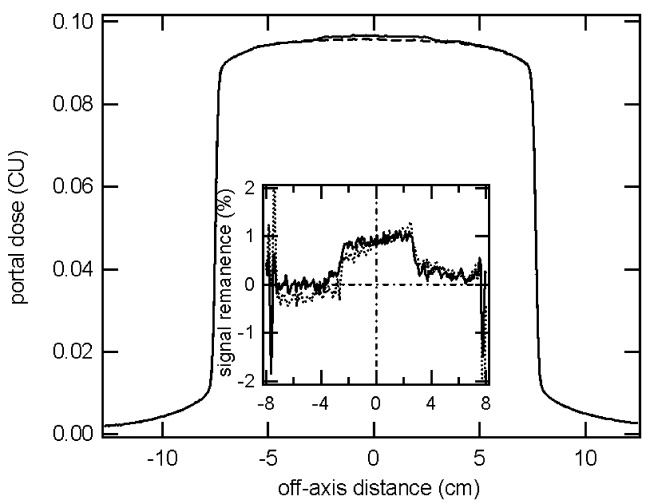

Fig. 4. Line profiles of the portal dose images of a 15×15 cm^2 static field (6 MV, 10 MU) with (solid line) and without (dashed line) preceeding irradiation of a 5×5 cm^2 field (500 MU). The ratio of both line profiles is displayed in the insert for 6 MV (solid line) and 18 MV (dotted line).

Table 1
Dosimetric error estimates for different linac dose rate settings and the corresponding acquisition mode settings

	SDD = 145 cm				SDD = 105 cm		
	Acquisition time/frame (s)	Measured cts/frame	Extrapolated cts for 65th frame	Dosimetric error for 65 frames (%)	Extrapolated cts/frame	Extrapolated cts for 65th frame	Dosimetric error for 65 frames (%)
6 MV dose rate (MU/min)							
100	0.290	2412	3776	0	4600	7201	0
200	0.148	2398	5055	0	4573	9640	0.54
300	0.111	2635	6528	0	5025	12,449	1.3
400	0.124	3839	8917	0.36	7321	17,004	1.9
500	0.131	4952	11,152	0.96	9443	21,266	17
600	0.121	5492	12,936	1.4	10,473	24,668	25
18 MV dose rate (MU/min)							
100	0.290	1838	2877	0	3505	5487	0
200	0.148	1821	3839	0	3473	7321	0
300	0.111	2081	5156	0	3968	9832	0.69
400	0.131	3130	7048	0	5969	13,441	1.4
500	0.131	3945	89,292	0.0035	7561	17,027	1.8
600	0.121	4529	10,668	0.0089	8637	20,343	9.2

Counts per frame were measured at SDD = 145 cm for the standard frame acquisition. All other listed values are extrapolated from these measurements.

3.1.5. Field size dependence

The PD measured by the aSi detector on the beam axis as a function of field size is displayed in Fig. 5. All data are normalised to the signal acquired for a 10×10 cm^2 field. For 6 MV (Fig. 5a) all measurements show similar behaviour: the output factors as measured by the detector at SDD = 145 cm are consistent with the measurements at SDD = 105 cm. The data acquired for rectangular field sizes are plotted as a function of their corresponding equivalent square field size. The concept of equivalent square field sizes is applicable within an accuracy of 2% for the clinically useable field sizes. Within the considered field size range, the dose to water shows comparable behaviour. For 18 MV (Fig. 5b), the same conclusions can be drawn with respect to the consistency of the aSi behaviour as a function of field size. However, discrepancies up to 9% are observed when comparing the field size dependence of the imager to the ionisation chamber measurements in water.

To fit the field size behaviour for each energy, we have used a second order polynomial. Combining the calibrated PD per MU on the beam axis as a function of field size (X,Y) and SDD into a single equation yields the output factor OF_{PI}

$$OF_{PI}(X, Y, SDD) = 0.01\left(\frac{100}{SDD}\right)^2 (a_0 + a_1 EFS + a_2 EFS^2) \quad (4)$$

with EFS the equivalent square field size and the fit parameters ($a_0 = 0.850$, $a_1 = 0.0176$ cm^{-1}, $a_2 = -0.288 \times 10^{-3}$ cm^{-2}) for 6 MV and ($a_0 = 0.779$, $a_1 = 0.0264$ cm^{-1}, $a_2 = -0.446 \times 10^{-3}$ cm^{-2}) for 18 MV. The factor 0.01 arises from the fact that the PD is calibrated to be unity for a total delivery of 100 MU at SDD = 100 cm, for a 10×10 cm^2 field.

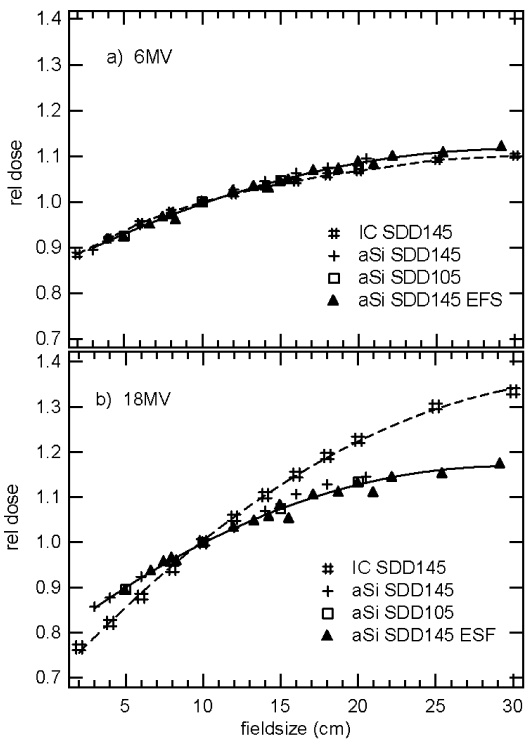

Fig. 5. Field size dependence of the signal on the beam axis, measured with an ionisation chamber (IC) in water (at 8 mm depth and SDD = 145 cm) and with the aSi detector for square as well as rectangular field sizes, at SDD = 105 and 145 cm. Measurements for 6 MV (a) and 18 MV (b) are plotted. All data series are normalised to their measurement for the 10×10 cm^2 field. Portal dose measurements for rectangular field size are plotted as a function of their corresponding equivalent square field size ESF. The dashed and solid lines represent the polynomial fits through the water and aSi measurements, respectively.

3.1.6. Portal depth dose

The dose measurements as a function of absorbing material are normalised to their maximum value: Fig. 6 displays these tissue maximum ratios (TMR) for 6 and 18 MV. For both energies, the PD behaviour deviates significantly from the dose to water measurement: the dose maximum is obtained at shallower depths for the PD measurements compared to the ionisation chamber measurements in water. In addition, the dose maximum plateau region is wider in the aSi measurement series: widths of ~1.5 and ~3 cm were observed for 6 and 18 MV, respectively.

3.2. Portal dose image prediction

Although the empirical fit parameters of the RF_{PI} (Table 2) show variations for different energies as well as for different imager distances, they all show similar components with corresponding weight factors of the same order of magnitude. A relative weight of ~96% is assigned to the narrow component ($k_1 < 1$ mm), ~4% of

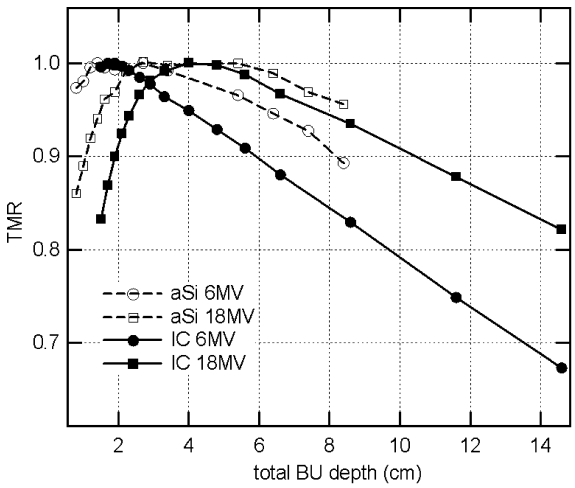

Fig. 6. Tissue maximum ratio for 6 and 18 MV measured with the aSi (open symbols) and with an ionisation chamber in water (closed symbols) at SDD = 145 cm. The 8 mm water equivalent thickness of aSi detector material was added to the amount of polystyrene to obtain the displayed total water equivalent build-up depth.

Table 2
Empirical fit parameters for the Gaussian functions in Eq. (3) from which the discrete kernels are sampled

	w_1	k_1 (mm)	w_2	k_2 (mm)	w_3	k_3 (mm)
6 MV SDD = 105 cm	0.960	0.015	0.033	4.9	0.007	21
6 MV SDD = 145 cm	0.959	0.015	0.033	4.5	0.008	25
18 MV SDD = 105 cm	0.967	0.018	0.027	5.9	0.006	24
18 MV SDD = 145 cm	0.964	0.017	0.027	4.3	0.009	28

Fit parameters are shown for both energies and for SDD = 105 and 145 cm.

the incoming fluence is scattered over a range in the order of a few mm (according to the second component k_2), the remaining component k_3 of $\sim 1\%$ describes a long range scatter of several centimetre. The thus obtained correspondence between measured and predicted PDs for the test fluence is visualised through the line profile in Fig. 7, e.g. for 6 MV at SDD = 105 cm.

In parallel with the gamma evaluation images—quantifying the overall correspondence—line profile comparisons illustrate the agreement between absolute PD prediction and measurement of the clinical IMRT fields (Fig. 8). Three examples are shown with varying degrees of intensity modulation and field size. The obtained data were within the postulated acceptance criteria, i.e. a conformity index of more than 95% was obtained for all fields for a maximum local dose difference of 3% and DTA of 3 mm. The points not meeting the acceptance criteria were evenly distributed over the whole field, implying that no errors of significant size could be found.

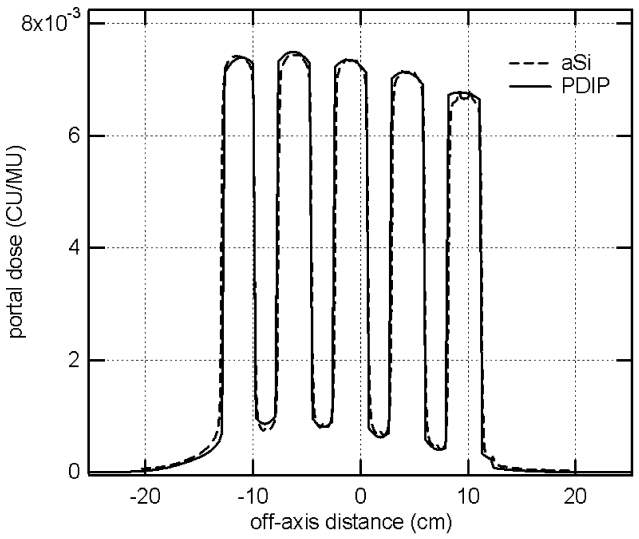

Fig. 7. Line profile through the measured and predicted portal dose distribution of the pyramid-like test fluence (Fig. 1), after optimisation of the discrete portal imager response function. The displayed example is obtained with 18 MV at SDD = 105 cm. (The small spikes at the dose peak at +10 cm are due to the fact that a substantial fraction of this dose peak is delivered through leaf transmission, making the interleaf transmission pattern distinguishable).

4. Discussion

4.1. Basic dosimetric characteristics of the aSi-based EPID

Although detector saturation is absent or negligible for all dose rate settings when measurements are performed at SDD = 145 cm, it introduces errors for dose rates beyond 200 MU/min for SDD = 105 cm. When the error is only the result of saturation of the 65th frame it is hardly noticeable in most clinical IMRT fields. However, dose rates for which saturation of all frames occurs should not be used for portal dosimetry. Although, for static field delivery, one could in theory attempt to correct for the overall dose underestimation, this is simply not possible for dynamic IMRT fields since the dosimetric information that was lost is time dependent and cannot be reconstructed. Although the presented results will deviate for linear accelerators that have been calibrated differently, one can state that, as a general guideline to avoid or reduce saturation effects, portal dosimetry can be performed with good accuracy ($<1.3\%$) at all SDD's by restricting linac dose rate settings up to 300 MU/min.

The dosimetric acquisition mode has shown to integrate all deposited dose, down to a delivery of 2 MU. The gradual decrease in accuracy beyond 2% for very low monitor units is mostly linked to the limited number of digits in the dosimetric workspace and therefore of little clinical relevance since, for dynamic as well as multiple static segment delivery, an IMRT field is delivered as one entity by the Varian accelerators and no (small) segments with few monitor units are measured individually.

There is no experimental evidence of a significant deviation from the inverse square law behaviour resulting from the increased contribution of the phantom scatter factor as the effective field size opening at the level of the detector surface is increased with increasing SDD (Fig. 3). The same behaviour is observed in ionisation chamber measurements in water at a depth of 8 mm: the gain in dose on the beam axis due to an increased phantom scatter contribution is possibly compensated for by the loss of contamination electrons with increased SDD. Hence, for the PD prediction, the aSi output factor for a $10 \times 10\ \text{cm}^2$ reference field as a function of SDD is modelled through the inverse square law behaviour.

Short as well as long term reproducibility of the PD detection were found to be excellent, consistent with data presented in literature [6,14]. Four-monthly dosimetric calibration of the detector showed to be sufficient for retaining the absolute reproducibility within 2% accuracy, but should intermediate dark and flood field corrections be performed, it is also recommended to redo the absolute calibration. This absolute dosimetric calibration requires only a single measurement of a reference field with the portal imager and is thus achieved in a matter of minutes.

Although a ghosting effects could be of concern for the imager in visual as well as dosimetric mode, these effects

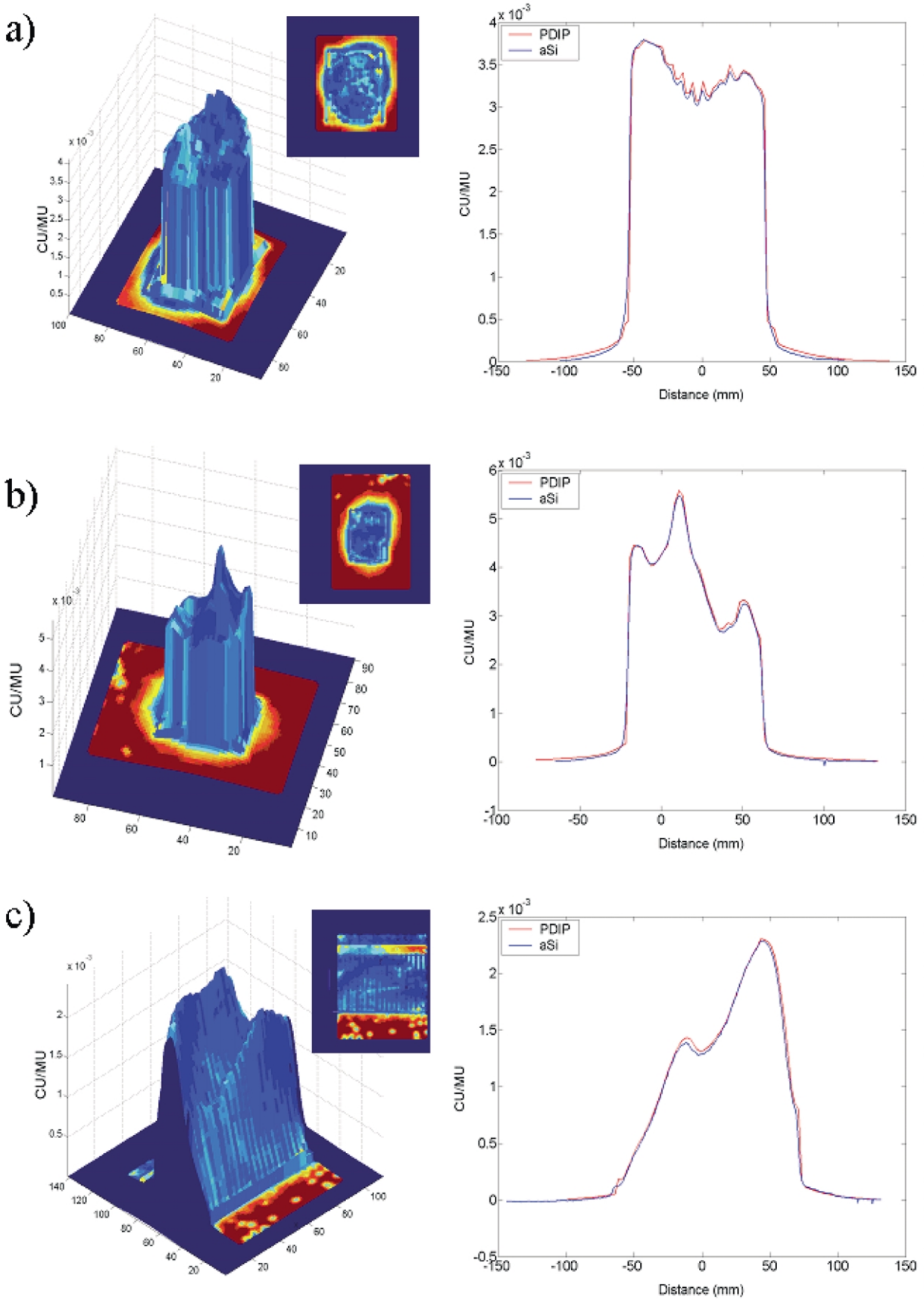
a)
b)
c)
CU/MU
x 10^-3
PDIP
aSi
Distance (mm)

could only be detected under extreme conditions, and no evidence of clinical relevance could be produced.

Although direct aSi detectors have been shown to exhibit similar behaviour to ionisation chamber measurements [4], this behaviour does not hold for the indirect aSi detector as has been shown previously [4] and can be concluded from the output factor and TMR measurements. The aSi TMR curves deviate significantly from the corresponding measurements in water for both energies, exhibiting a wider plateau and slower fall-off. Considering the results published by El-Mohri et al. [4] on a direct aSi detector construction, we conclude the observed differences to be due to the enhanced sensitivity of the phosphor scintillator to the low energy components in the incident radiation spectrum, more specifically to contamination electrons and to low energy photons and electrons created through interaction of the primary photons with the build-up material. Although further fundamental investigations, such as extended Monte Carlo calculations, will be useful in further explaining or quantifying the observed behaviour, important conclusions can already be drawn:

Firstly, the aSi response is not linear with dose to water as measured by, e.g. ionisation chamber. The ionisation chamber measurements are displaying the behaviour of the dose to water, the aSi measurements are merely displaying the integrated response of the portal imager to the incoming fluence: the PD is not equivalent to the dose to water, as demonstrated by the field size dependent measurements and the TMR data.

Secondly, although measuring in a high gradient region is not standard practice, the authors believe that adding build-up to the detector surface will neither facilitate nor complicate the prediction of the PD. Even if not accurately known, the depth is accurately fixed. In addition, other practical arguments discourage the use of supplementary build-up slabs onto the detector cover since the primary goal of our work is to maximise efficiency in the clinical routine. Since the manufacturer is not inclined to incorporate build-up into the commercial EPID design, adding build-up would compromise the achievement of this goal since it would require an interlock override on the collision detection of the imager and it would inhibit PD image acquisition at non-zero gantry positions, i.e. at the actually planned gantry rotations. So, although the measurements performed by the unaltered, commercially available aSi portal imager are always obtained at a high gradient region with respect to the build-up depth, this does not pose a problem since the thickness of the internal build-up layer is small but mechanically fixed, leading to reproducible data, regardless of precise thickness.

Although the aSi is not an ionisation chamber equivalent detector, its field size dependent behaviour is self-consistent at different source to detector distances and because of the demonstrated applicability of the concept of an equivalent square field size, the field size dependence of the aSi can be modelled through a single analytical fit function.

4.2. Portal dose prediction

The accuracy of the derived RF_{PI} is decisive for the quality of the PD image prediction. The discrete RF_{PI} as derived from a least square fit of a measurement versus PD prediction showed satisfactory results. The fact that slightly different parameter values have to be used for the analytical function from which the discrete RF_{PI} is constructed at different SDD, confirms the critical impact of the sampling resolution. The consistent appearance of a long-range component in the RF_{PI} is in correspondence with the so-called glare effect [14]. A long-range component should be present due to brehmsstrahlung and scattered photon radiation generated in the detector itself, which McCurdy et al. modelled via Monte Carlo simulation, and possibly an additional optical glare component, which McCurdy et al. were not able to model through Monte Carlo, but through a fit on the empirical data. The true nature of this optical glare effect is possibly related to the presence of the glass substrate holding the active aSi layer [17] but needs further investigation.

Using the empirically derived discrete RF_{PI} and the aSi specific output factors, the presented algorithm allows absolute PD prediction for pre-treatment QA applications within an accuracy of 3% of the local dose and 3 mm distance to agreement within the area defined by the 5% isodose line (with respect to the maximum PD per field).

5. Conclusions

The aSi (aS500) EPID proves to be a convenient and accurate detector for static as well as dynamic portal dosimetry, when operated in the dose acquisition mode. Although the behaviour of the aSi detector is not equivalent to a dose to water measurement, it is self-consistent and reproducible. Hence, an absolute PD image prediction could be developed allowing verification of the actual fluence delivery of individual IMRT fields. When comparing the

Fig. 8. Gamma evaluation and line profile comparisons for three clinical IMRT fields of varying field size and intensity modulation, treatment energy and SDD: (a) small IMRT field for irradiation of a local recurrence (18 MV, SDD = 105 cm), (b) IMRT prostate field (6 MV, SDD = 105 cm) and (c) subfield of a multiple carriage IMRT delivery for a head and neck treatment (6 MV, SDD = 145 cm). Gamma evaluations are displayed in two modes: the 3D representations display the portal dose prediction in 3D and coloured according to the corresponding gamma index for each point. All shades of blue are within the acceptance criteria. Colours evolving from yellow to red have an increasingly large gamma value (ranging from 1 to 3). Additionally, the insert shows a 2D beams-eye-view of the gamma evaluation with the same colour scale. The position of the line profiles was chosen in order to represent the degree of modulation.

acquired integrated images to the PD distribution calculated by the prediction algorithm, acceptance criteria of 3% dose difference and 3 mm DTA were met (with a conformity index of more than 95%) for all tested IMRT fields.

Portal dosimetry provides a tool for routine, pre-treatment QA of IMRT treatments that is potentially significantly faster and more convenient than current pre-treatment methods.

Acknowledgements

The authors would like to thank Dr D. Vetterli and Dr P. Manser from Inselspital (Bern, Switzerland) and Dr P. Storchi and M. de Langen from Daniel den Hoed Cancer Centre (Rotterdam, The Netherlands) for fruitful discussions. This work was supported by Varian Medical Systems. T. Depuydt was sponsored by the European Commission (ESQUIRE project).

References

[1] Boellaard R, Van Herk M, Uiterwaal H, Mijnheer BJ. Two-dimensional exit dosimetry using a liquid-filled electronic portal imaging device and a convolution model. Radiother Oncol 1997;44: 149–59.

[2] Chang J, Mageras GS, Chui CS, et al. Relative profile and dose verification of intensity modulated radiation therapy. Int J Radiat Oncol Biol Phys 2000;47(1):231–40.

[3] Depuydt T, Van Esch A, Huyskens DP. A quantitative evaluation of IMRT distributions: refinement and clinical assessment of the gamma evaluation. Radiother Oncol 2002;62:309–19.

[4] El-Mohri Y, Antonuk LE, Yorkston J, et al. Relative dosimetry using active matrix flat-panel imager (AMFPI) technology. Med Phys 1999; 26:1530–41.

[5] Essers M, Boellaard R, van Herk M, Lanson JH, Mijnheer BJM. Transmission dosimetry with a liquid-filled electronic portal imaging device. Int J Radiat Oncol Biol Phys 1996;34:931–41.

[6] Greer PB, Popescu CC. Dosimetric properties of an amorphous silicon electronic portal imaging device for verification of dynamic intensity modulated radiation therapy. Med Phys 2003;30:1618–27.

[7] Haas B, Mey L, Andre L. Generation of inhomogeneous irradiation fields by dynamic control of multileaf collimators. MSc Thesis, University of Bern; 1996.

[8] Heijmen BJM, Pasma KL, Kroonwijk M, et al. Portal dose measurement in radiotherapy using an electronic portal imaging device (EPID). Phys Med Biol 1995;40:1943–55.

[9] Kausch C, Schreiber B, Kreuder F, Schmidt R, Dössel O. Monte Carlo simulations of the imaging performance of metal plate/phosphor screens used in radiotherapy. Med Phys 1999;26:2113–24.

[10] Low DA, Harms WB, Sasa M, Purdy JA. A technique for the quantitative evaluation of dose distributions. Med Phys 1998;25: 656–61.

[11] Ma L, Geis PB, Boyer AL. Quality assurance for dynamic multileaf collimation system using a fast beam imaging system. Med Phys 1997;24:1213–20.

[12] Manser P, Bühlmann R, Fix MK, Vetterli D, Mini R, Rüegsegger P. Calculations and measurements of portal dose images in IMRT. Med Phys 2001;28:1267.

[13] Manser P, Treier R, Riem H, et al. Dose response of an aSi:H EPID on static and dynamic photon beams. Med Phys 2002;29:1269.

[14] McCurdy BMC, Luchka K, Pistorius S. Dosimetric investigation and portal dose image prediction using an amorphous silicon electronic portal imaging device. Med Phys 2001;28(6):911–24.

[15] McCurdy BMC, Pistorius S. A two-step algorithm for predicting portal dose images in arbitrary detectors. Med Phys 2000;27: 2109–16.

[16] McNutt TR, Mackie TR, Reckwerdt P, Papanikolaou N, Paliwal BR. Calculation of portal dose using the convolution/superposition method. Med Phys 1996;23:527–35.

[17] Munro P, Bouius DC. X-ray quantum limited portal imaging using amorphous silicon flat-panel arrays. Med Phys 1998;25:689–702.

[18] Pasma KL, Heijmen BJM, Kroonwijk M, Visser AG. Portal dose image (PDI) prediction for dosimetric treatment verification in radiotherapy. I. An algorithm for open beams. Med Phys 1998;25: 830–40.

[19] Pasma KL, Kroonwijk M, de Boer JCJ, Visser AG, Heijmen BJM. Accurate portal dose measurement with a fluoroscopic electronic portal imaging device for open and wedged beams and dynamic multileaf collimation. Phys Med Biol 1998;43:2047–60.

[20] Pasma KL, Dirkx MLP, Kroonwijk M, Visser AG, Heijmen BJM. Dosimetric verification of intensity modulated beams produced with dynamic multileaf collimation using an electronic portal imaging device. Med Phys 1999;26(11):2373–8.

[21] Spies L, Bortfeld T. Analytical scatter kernels for portal imaging at 6 MV. Med Phys 2001;28:553–9.

[22] Storchi P, Woudstra E. Calculation of the absorbed dose distribution due to irregularly shaped photon beams using pencil beam kernels derived from basic input data. Phys Med Biol 1996;41:637–56.

[23] Van Esch A, Vanstraelen B, Verstraete J, Kutcher GJ, Huyskens DP. Pre-treatment dosimetric verification by means of a liquid-filled electronic portal imaging device during dynamic delivery of intensity modulated treatment fields. Radiother Oncol 2001;60:181–90.

[24] Van Esch A, Bohsung J, Sorvari P, et al. Acceptance tests and quality control procedures for the clinical implementation of intensity modulated radiotherapy (IMRT) using inverse planning and sliding windows technique: experience from five radiotherapy departments. Radiother Oncol 2002;65:53–70.